Progression of Aortic Dissection: An Application of Soliton Solutions of Nonlinear Evolution Equation in (3+1)-Dimensions

VISHAKHA JADAUN (vishakhasjadaun@gmail.com)
Netaji Subhas University of Technology
Nitin Singh
Indian Institute of Technology Delhi

Research Article

Keywords: Aortic dissection, Soliton Solutions, Nonlinear Evolution Equation , dynamic pathology

Posted Date: November 3rd, 2021

DOI: https://doi.org/10.21203/rs.3.rs-1029184/v1

PROGRESSION OF AORTIC DISSECTION: AN APPLICATION OF SOLITON SOLUTIONS OF NONLINEAR EVOLUTION EQUATION IN (3+1)-DIMENSIONS

VISHAKHA JADAUN* AND **NITIN RAJA SINGH**

Abstract. Aortic dissection is a serious pathology involving the vessel wall of the aorta with significant societal impact. To understand aortic dissection we explain the role of the dynamic pathology in the absence or presence of structural and/or functional abnormalities. We frame a differential equation to evaluate the impact of mean blood pressure on the aortic wall and prove the existence and uniqueness of its solution for homeostatic recoil and relaxation for infinitesimal aortic tissue. We model and analyze generalized (3+1)-dimensional nonlinear partial differential equation for aortic wave dynamics. We use the Lie group of transformations on this nonlinear evolution equation to obtain invariant solutions, traveling wave solutions including solitons. We find that abnormalities in the dynamic pathology of aortic dissection act as triggers for the progression of disease in early-stage through the formation of soliton-like pulses and their interaction. We address the role of unstable wavefields in waveform dynamics when waves are unidirectional. Moreover, the notion of dynamic pathology within the domain of vascular geometry may explain the evolution of aneurysms in cerebral arteries and cardiomyopathies even in the absence of anatomical and physiological abnormalities.

1. Introduction

Aortic dissection is a life threatening condition caused by tear in the tunica intimal layer of the aorta resulting into separation of the layers of the aortic wall. In elderly population, incidence of this catastrophic disease is 36 cases per 100,000 people per year. The dynamic pathology underlying aortic dissection can be evaluated using nonlinear evolution equations (NLEEs) explaining perturbation, development and dispersion including nonlinear effects. NLEEs have been used to explore varied nonlinear phenomena present in scientific inquiry domain including its technological perspective. Various methods [1–8] such as the inverse scattering transformation, Bácklund transformation, $(\frac{G'}{G})$-expansion method, Darboux transformation and Hirota method have been proposed to solve the NLEEs. Traveling wave solutions including soliton have been implicated to understand complex physical, chemical and biological phenomena. Herein, we peruse soliton interaction as precursor for genesis of unstable wave field that contributes to dynamic pathology in aortic dissection.

This paper is organized in the following manner. Section 2 presents background of aortic dissection and NLEEs including public health relevance, rationale for the model, a primer on disease, wave form dynamics in normal aorta and dynamic pathology in aortic dissection; and a primer on NLEEs & soliton solutions. Section 3 presents mathematical model to evaluate impact of pressure reaction force of hemodynamics on vessel wall of the aorta. We solve boundary value problem for mean blood pressure and proved uniqueness and existence of its solution. We also formulate a generalized (3+1)-dimensional nonlinear evolution equation to model dynamic pathology of aortic wave forms. Section 4 outlines Lie group of transformations method for system of partial differential equations. Section 5 describes about symmetry reduction and soliton solutions for generalized $(3+1)$-dimensional NLEE. Along with, We discuss soliton solutions using graphic interpretation. Lastly, Section 6 presents conclusion and future scope.

2. Biological Background of Aortic Dissection

2.1. **Public Health Relevance.** Aortic dissection is the most common catastrophic disease affecting aorta [9,10]. Incidence of acute aortic syndromes recorded at emergency department in hospitals is three-five per 100,000 people per year [11–15].

Key words and phrases. Nonlinear Dynamics; Nonlinear evolution equations; Lie group of transformations; Soliton; Aortic dissection.

Since hospital-based case accounting fails to include pre-admission deaths related to complications from aortic dissection [16–20], this figure underestimates the actual incidence rate of acute dissection. A prospective analysis of 30,412 middle-aged population with a mean twenty years follow-up reported fifteen cases per 100,000 patients per year are at risk of aortic dissection. Note that patient accounting at hospitals reveals male preponderance, women with aortic dissection presents late at an older age since symptoms are atypical. Thus, women with aortic dissection have higher pre-admission mortality owing to complications from aortic dissection. In older age group, 65-75 years of age, the incidence might be even higher, thirty-six cases per 100,000 per year.

2.2. **Rationale for the model.** Aortic dissection poses a special diagnostic challenge for cardiothoracic physicians and vascular surgeons because of its relative rarity. Its clinical presentation is highly variable and mimics other more common non-cardiovascular conditions.

- Note that accurate measurements of aortic dimension are difficult to obtain because the aorta is a complex geometrical structure. Though standardized measurements made perpendicular to the axis of blood flow are important to assess changes in aortic size over time and to avoid erroneous findings of arterial growth, inter-observer and intra-observer variability in measurements of aneurysm diameter on CT imaging have been shown to be 5 mm and 3 mm, respectively [14, 15]. Thus, any change of 5 mm on a serial CT evaluation can be considered a significant change, but smaller changes (including systolic and diastolic features) are difficult to interpret.

- In contrast to CT, ultrasonographic techniques underestimate aortic dimensions by an average of 13 mm; thus, the same imaging technique should be used for serial measurements in any given patient. Specific features that relate to management decisions are important, such as the presence of rupture, the extent of the dissection, the involvement of branch vessels and end-organ ischemia.

- There are no reports on cellular and molecular differences between dissections affecting ascending and descending aorta. This paper develops new mathematical model for aortic dissection, wherein blood permeates in between layers of vessel wall of the aorta, allowing for the formation of parallel flow paths within the vessel. The model can be used to study fundamental questions about aortic dissection and its clinical management. Such a model ultimately promises to aid in clinical decision making by determining the optimal choice and timing of medical and surgical approaches to treating aortic dissection.

Thus, the correct diagnosis is missed on initial presentation and delayed in $> 30\%$ of cases [9]. Prompt diagnosis is important since mortality and long-term morbidity are related to late implementation of therapeutic regimen including risk reduction therapy. Clinical imaging, disease biomarkers and genetic predisposition are keys to understand the risk of developing an aortic dissection, confirm a suspected diagnosis and determine the appropriate therapeutic intervention for a particular patient.

2.3. **A primer on disease: Aortic dissection.** Acute aortic dissection is characterized by rapid progression of disease with development of initial flap owing to injury by flowing blood to tunica intima and blood permeating into tunica media, forcing tunica intima and tunica adventitia apart. As disease progress further, blood continue to permeate within tunica media and extend in both antegrade as well as retrograde direction from site of initial lesion. Note that such extension can involve arterial branches emanating from aorta.
Generally acute stage lasts for fourteen days wherein patient is highly susceptible to life threatening complications such as sudden rupture and concomitant torrential bleed leading to sudden death. This is followed by subacute stage lasting for ninety to one hundred days wherein aortic tissue undergoes remodeling. Then, chronic stage ensues. The complications with potential catastrophic outcomes including ischemia to vital organs, aortic valvular regurgitation & insufficiency, pericardiac tamponade, sudden aortic rupture, circulatory failure & cardiogenic shock and death.

To enable therapeutic decisions, aortic dissection is classified on the basis of anatomic topographic classification system. It also accounts for location of separation of layers and extent of dissection. Stanford type A (DeBakey type I and type II) aortic dissection involves ascending aorta including arch of aorta. Stanford type B (DeBakey type IIIa and type IIIb) aortic dissections involving descending aorta [9, 10].

2.4. **Waveform dynamics in normal aorta.** As an elastic artery, aorta is complaint to propagate wave of blood flow. It is a highly complex nonlinear phenomenon including wave interference, resonance and other interactions. The wave propagation and reflection in aorta create wave dynamics wherein dynamics depends upon biomechanical properties of compliant tube; frequency of central left ventricular contraction and peripheral vascular recoil; and location of reflection sites as in complex geometry of ascending, arch and descending aorta [21–27]. Note that such wave dynamics promotes blood flow in one direction while retarding the flow in other direction. The magnitude of flow dynamics exhibits nonlinear dynamic behavior [28].

2.5. **Dynamic pathology in aortic dissection.** Dynamic pathology is characterized by a quasi-steady state. Dynamics of cardiovascular system are deviated from the homeostatic condition. Note that anatomical and physiological dysfunctional states can be concomitantly present. It means that mere absence of anatomical and physiological dysfunctional states doesn't exclude the possibility of existence of dynamic pathology [29]. The dynamic pathology can contribute to progression of aortic dissection by either functioning as a trigger to initiate anatomical and/or physiological disturbance or acting persistently over the disease course. Also, concurrence of anatomical and physiological dysfunctional states with dynamic pathology is responsible for catastrophic events such as rupture of aneurysmal sac, torrential bleed and sudden death.

2.5.1. *Pathological waves: Creation of wave field.* One of essential complications in the dynamic pathology of aortic dissection is the existence of more than one horizontal spatial coordinates for interference among solitary waves creating a meta-stable wave field. The directional behavior of these waves in the dynamic pathology consists of formation of unstable wave field, wherein many waves crossing each other at various angles. At a linear scale, it can be summed up as the pathological wave inclusive of long-crested and short-crested waveforms emerging from different directions [30–33]. Under abnormal anatomical and/or physiological states, these waveforms harbours destructive characteristics and contribute to the dynamic pathology with/without structural and/or functional interplay between heart and aorta. On long-term basis, the dynamic pathology introduces transient to permanent structural abnormalities in vessel wall of aorta. Solitons and breathers are nonlinear solitary wave entities that propagate at an angle with respect to the propagation of the wave field. Note that in nonlinear dynamics, these waveforms have dynamic interactions including constructive & destructive features and interference & resonance behavior.

2.5.2. *The negative effects of the dynamical pathology on aortic vessel wall.* The aortic waves act destructively and impedes the forward flow and counterintuitively pushes blood in opposite direction. It has two implications: firstly, it increases cardiac workload by defective aortic valvular regurgitation; and secondly, aortic compression waves and suction waves are created with every cardiac cycle. Aortic compression waves and suction waves anomalously impacts aortic vessel wall.

2.5.3. *Hypothesis.* We propose that abnormalities in the dynamic pathology of aortic dissection act as triggers for progression of disease in early stage through formation of wave field and interaction therein. Addressing the role of second coordinate to the wave form dynamics when waves are unidirectional is essential.

2.6. **Nonlinear Evolution Equations and Soliton Solutions.** Nonlinear evolution equations (NLEEs) have been perused to address nonlinear phenomena in various branches of sciences [34–39] including biology and medicine. NLEE explains permeation of two-layer fluid comprised of blood and hypoxia inducible factor - 1α in dispersive media. It also explains the behaviour of bubbly fluids and causation of cerebral arterial gas embolism. Moreover, the nonlinear blood flow in proximal aorta can be modeled as flows over an inclined plane using NLEE. Research on NLEEs solutions including solitary waves and solitons remains most vibrant area in mathematics and physics.
A soliton is a solitary wave that arises from a delicate balance between nonlinear and dispersive effects. It maintains its shape while moving at the constant speed and its pulse width depends on the amplitude. For a non-dissipative system, a soliton is

solitary wave whose amplitude, shape and velocity are conserved. A soliton collide with another soliton, their fundamental parameters remain conserved except phase shift [40, 41]. Bright soliton refers to a soliton that causes a temporary increment in an associated wave amplitude than the background, whereas dark soliton refers to a soliton whose intensity is smaller than the background, instead it essentially lack of energy in a continuous time beam. A bright soliton with a classic double spatio-temporal localization is Peregrine soliton. It seems to be an appealing hypothesis to explain formation, progression and decay of such chaotic wave which suddenly develops high amplitude and concomitant narrowing of temporal duration. Breather is a soliton with energy concentrated in an oscillatory and localized manner. Discrete breathers are extremely spatially localized time pervasive excitations in spatially extended, discrete and periodic system [42]. The multi-soliton complex is a self-localized state. It emerges from nonlinear superimposition various fundamental solitons including bright soliton and dark soliton. This superimposition among various solitons might be either incoherent or coherent depending upon the phases of the separate solitons.

3. Mathematical Formulations

3.1. **Vessel Wall of Aorta.** To derive the model for dynamic pathology of the aortic dissection, we consider the motion of vessel wall of aorta. Consider the elastic artery as a circularly cylindrical elongated tube with radius R_0. Assume that the elastic artery is a thin-walled incompressible axially prestretched hyperelastic tube with a localized axially symmetric dilatation with tunica intima flap injury. This elastic artery is subjected to initial axial stretch π and a uniform pressure inside aortic wall $\mathcal{E}_0(\mathfrak{z})$ For a healthy human, systolic blood pressure is 120 mm Hg and diastolic blood pressure is 80 mm Hg. Mean blood pressure is 100 mm Hg. The position vector of a given point on the elastic artery is given by

$$\vec{\mathfrak{r}_0} = [\mathfrak{r}_0 + \mathfrak{f}(z)]e_{\mathfrak{r}} + ze_z,\ z = \pi\ \mathfrak{z}, \tag{3.1}$$

where e_z and e_r are the unit basic vectors in the cylindrical polar coordinates, $\mathfrak{r}_0$ is the deformed radius at the origin of the cylindrical polar coordinate system, $\mathfrak{z}$ is the axial polar coordinate before the deformation of the elastic artery, z is the axial polar coordinate after the static deformation of the elastic artery, $\mathfrak{f}(z)$ is a function to describe the geometry of nonlinearly dilated aortic dissection. After application of the initial static deformation, we shall superimpose only a dynamical radial displacement $u(z,t)$ to the initial static deformation, then the position vector $\vec{\mathfrak{r}}$ of a given point on the elastic artery is given by

$$\vec{\mathfrak{r}} = [\mathfrak{r}_0 + \mathfrak{f}(z) + u(z,t)]e_{\mathfrak{r}} + ze_z. \tag{3.2}$$

Note that the axially prestreched artery does not undergo significant deformation after application of initial static deformation. The longitudinal motion of arteries is also quite small because of strong vascular tethering as well as helical circumferential orientation of the elastin and collagen fibers. The arc-lengths along meridional and longitudinal curves respectively are as follows

$$dS_z = \left[1 + \left(\frac{d\mathfrak{f}}{dz} + \frac{\partial u}{\partial z}\right)^2\right]^{\frac{1}{2}} dz,\ dS_\theta = [\mathfrak{r}_0 + \mathfrak{f} + u]d\theta. \tag{3.3}$$

The stretch ratios in the longitudinal and circumferential directions in the final configuration are presented

$$\pi_1 = \pi\Upsilon,\ \pi_2 = \frac{1}{R_0}(\mathfrak{r}_0 + \mathfrak{f} + u),\ \text{where } \Upsilon = \left[1 + \left(\mathfrak{f}' + \frac{\partial u}{\partial z}\right)^2\right]^{\frac{1}{2}} \tag{3.4}$$

The notation $(\prime)$ denotes the differentiation of $\mathfrak{f}$ with respect to z. Then, the unit tangent vector $\mathfrak{t}$ along the deformed meridional curve and the unit normal vector $\mathfrak{n}$ to the deformed tube after application of static deformation are expressed by

$$\mathfrak{t} = \frac{\left(\mathfrak{f}' + \frac{\partial u}{\partial z}\right)e_{\mathfrak{r}} + e_z}{\Upsilon},\ \mathfrak{n} = \frac{e_{\mathfrak{r}} - \left(\mathfrak{f}' + \frac{\partial u}{\partial z}\right)e_z}{\Upsilon} \tag{3.5}$$

According to the assumption made about the aortic vessel wall material incompressibility, the following restriction holds:

$$\delta = \frac{\Delta}{\pi_1 \pi_2}, \tag{3.6}$$

where Δ and δ are the vessel wall thickness before and after deformation, respectively. The force that acts on the infinitesimal aortic wall component placed between the planes $z = A_1$, $z + dz = A_2$, $\theta = A_3$ and $\theta + d\theta = A_4$, where A_i, $i = 1, \ldots, 4$ are arbitrary constants.
This determines its motion

$$\mathbf{F} = -T_2 \Upsilon \left\{ \frac{(\mathfrak{r}_0 + \mathfrak{f} + u)\left(\mathfrak{f}' + \frac{\partial u}{\partial z}\right) T_1}{\Upsilon} \right\} + \mathcal{E}(\mathfrak{r}_0 + \mathfrak{f} + u)\Upsilon, \tag{3.7}$$

where $\mathcal{E}$ is the fluid reaction force.
T_1 and T_2 are tensions in the longitudinal and circumferential directions given by

$$T_1 = \frac{\mu \Delta}{\pi_2} \frac{\partial \Psi}{\partial \pi_1}, \; T_2 = \frac{\mu \Delta}{\pi_1} \frac{\partial \Psi}{\partial \pi_2}, \tag{3.8}$$

where Ψ is the strain energy density function of the wall material and μ is the material shear modulus.
Finally, the equation of the radial motion of infinitesimal segment of vessel wall of the aorta is given by

$$\frac{\mu}{\pi} \frac{\partial \Psi}{\partial \pi_2} + \mu R_0 \frac{\partial}{\partial z} \left\{ \frac{\left(\mathfrak{f}' + \frac{\partial u}{\partial z}\right)}{\Upsilon} \frac{\partial \Psi}{\partial \pi_1} \right\} + \frac{\mathcal{E}}{\Delta}(\mathfrak{r}_0 + \mathfrak{f} + u)\Upsilon = \rho \frac{R_0}{\pi} \frac{\partial^2 u}{\partial t^2}, \tag{3.9}$$

where ρ is the mass density of the tube material.
Above equation models aorta as an elastic artery that is axially prestrechted hyperelastic tube. Note that the elastic properties of the injured wall differs from the healthy part. We assume that the wall is homogeneous. Thus, material shear modulus μ is constant. Now the above equation holds equivalently valid for normal constitutive features of aorta. Further, we seek to assess the impact of mean blood pressure as pressure reaction force on vessel wall of aorta including the tunica media. In the next subsection, we formulate a boundary value problem in this regard.

3.2. **Boundary Value Problem Related to Mean Blood Pressure.** The systolic blood pressure contributes to the flow of oxygenated blood in the arterial system through aorta. Diastolic blood pressure contributes to the flow of oxygenated blood to coronary microvasculature. The aorta is circularly cylindrical shaped tube with diameter approximately equals to 2.2 *cm*. We assume that the blood flow is incompressible and newtonian in aorta. Since we know that intermediate layer in the vessel wall of the aorta, the tunica media, is constituted of vascular smooth muscle cells and fibroblast within the boundary of internal and external elastic basal lamina. The blood flow ejected from left ventricle is propagated through aorta. The pressure reaction force applied by blood flow to the vessel wall of the aorta causes initial static deformation that continues distally with each left ventiricular contraction followed by aortic reflexive dilatation and consequent circumferential elastic recoil. Since the tunica intima is unicellularly thick, the pressure reaction force is directly passed onto tunica media. Since there is no diffusive flux from tunica intima to tunica media, the mean blood pressure follows Michaelis-Menten kinetics. Hence, the boundary value problem(BVP) for mean blood pressure is formulated as follows

$$\begin{aligned} Q''(r) &+ \frac{2}{r} Q'(r) = \frac{aQ(r)}{Q(r) + C} \\ Q'(0) &= 0, \quad Q'(1) = D(1 - Q(1)). \end{aligned} \tag{3.10}$$

where $Q(r)$ is mean blood pressure in homeostatic steady state, r is the volumetric flow rate and a, D,C are positive constants. Here, $(\prime)$ denotes differentiation with respect to r.

Theorem 1. *The BVP* (3.10) *has unique solution* $Q(r)$ *s.t.* $Q(0) \geq 0$. *The solution* $Q(r)$ *is strictly monotone increasing and* $Q(r) \leq 1$.

Proof. The initial value problem

$$Q'' = -\frac{2}{r}Q' + \begin{cases} \frac{aQ}{Q+K}, & Q \geq 0 \\ 0, & Q < 0 \end{cases} \tag{3.11}$$
$$Q'(0) = 0, \quad Q(0) = \alpha \quad (\alpha > 0)$$

has unique twice continuously differentiable solution [43]. Let $Q(r;\alpha)$ is a solution stressing its dependence on initial value α.

$$Q''(0;\alpha) = \frac{a\alpha}{\alpha + K} \tag{3.12}$$
$$\because \qquad \alpha \geq 0 \Rightarrow Q''(0;\alpha) > 0.$$

Consider there exist a zero of Q' in $[0,1]$, and let the smallest zero is β, then

$$Q'(r,\alpha) > 0, \quad \text{for} \quad 0 < r < \beta \tag{3.13}$$
$$\Rightarrow \quad Q(\beta,\alpha) > 0$$

From equation (3.11)

$$Q''(\beta;\alpha) > 0$$
$$\therefore \qquad \exists\ \varepsilon > 0 \quad s.t. \quad \beta - \varepsilon > 0 \quad \text{and} \quad Q'(\beta - \varepsilon, \alpha) < 0$$

which is a contradiction that β is the smallest zero.
Consequently,

$$Q'(r,\alpha) > 0, \quad \text{for} \quad 0 < r \leq 1 \tag{3.14}$$
$$Q(r,\alpha) > 0, \quad \text{for} \quad 0 \leq r \leq 1. \tag{3.15}$$

Here, It is clear that Q is monotone increasing

$$Q'(r,\alpha_1) > Q'(r,\alpha_2) \quad \text{for} \qquad 0 < r \leq 1 \tag{3.16}$$
$$Q'(r,\alpha_1) > Q'(r,\alpha_2) \quad \text{for} \qquad 0 < r \leq 1 \tag{3.17}$$

whenever $\alpha_1 > \alpha_2 > 0$.
From equation (3.11), we assume

$$f(r,Q,Q') = -\frac{2}{r}Q' + \begin{cases} \frac{aQ}{Q+K}, & Q \geq 0 \\ 0, & Q < 0 \end{cases} \tag{3.18}$$

The function $f(r,Q,Q')$ satisfies Lipschitz condition:

$$f(r,Q,Q') - f(r,\tilde{Q},\tilde{Q}') \leq \frac{a}{K} \cdot |Q' - \tilde{Q}'| \quad \text{for } Q'' \geq Q''. \tag{3.19}$$

$Q(1;\alpha)$ and $Q'(1;\alpha)$ are continuous functions [44], therefore the function

$$K(\alpha) = Q'(1;\alpha) - D(1 - C(1;\alpha)) \tag{3.20}$$

is strictly monotone increasing. The initial value problem (3.11) has trivial solution for $\alpha = 0$. Hence $K(\alpha) < 0$ because of equation (3.14). But $Q(r;1)$ is strictly monotone increasing. Therefore,

$$Q(1;1) > Q(0;1) = 1 \quad \Rightarrow K(1) \geq 0. \tag{3.21}$$

Hence, there exists unique positive solution $\overset{*}{\alpha}$ of $K(\alpha) = 0$. This implies that the BVP (3.10) possesses unique solution. □

3.3. **Equation for dynamical pathology in aortic dissection.** Since length of the aorta is very large in comparison to its radius and the axial-circumferential wave formed by the blood flow is relatively smaller than radius itself, NLEE is perused for modeling of these waveforms over the tunica intimal surface. Consider v as a holomorphic function of spatial coordinates (r, s, q) and temporal coordinate t that represents amplitude of resultant wave and it is complex differentiable at every point in $\mathbb{R}$. For a wave envelope $v(r, s, q, t)$ with wave number λ along with directions of r, s and q, we have

$$3u_{rq} - (2u_t + u_{rrr} - 2uu_r)_s + 2(u_r\partial_r^{-1}u_s)_r = 0 \tag{3.22}$$

We use transformation $v_r = u$ in Eq. (3.22) to obtain generalized form of $(3+1)$-dimensional NLEE amenable to similarity transformations method, is given by

$$\Delta := 3v_{rrq} - 2v_{rst} + v_{rrrrs} - 2v_{rs}v_{rr} + 2v_{rs}^2 + 2(v_s - v_r)v_{rrs} = 0, \tag{$\star$}$$

where v_{rst} and is the development term, v_{rrrrs} is dispersion term, $v_{rs}v_{rr}$, v_{rs}^2 & $(v_s - v_r)v_{rrs}$ are nonlinear terms and v_{rrq} is the linear term.

4. Lie Group of Transformations Method

In this section, we recall the general procedure for determining symmetries for any system of partial differential equations. Let us consider the general case of a system of partial differential equations of order p with $m-$dependent and $n-$independent variables, given as

$$\Delta_x(r, p^u) = 0, \qquad x = 1, \ldots, l. \tag{4.1}$$

Here $r = (r_1, r_2 \ldots r_n)$, $p = (p_1, p_2 \ldots p_m)$ and the derivatives of p with respect to r upto order u is denoted as p^u. We consider one parameter Lie group of infinitesimal transformations acting on dependent variable p and independent variable r of (4.1),

$$\left.\begin{aligned} \check{r^i} &= r^i + \varsigma\xi^i(r,p) + O(\varsigma^2), \quad i = 1, 2, \ldots, n \\ \check{p^j} &= p^j + \varsigma\eta^j(r,p) + O(\varsigma^2), \quad j = 1, 2, \ldots, m \end{aligned}\right\} \tag{4.2}$$

where ξ^i and η^j are generators of infinitesimal transformation for the independent and dependent variables respectively and ς is the group parameter which is admitted by the system (4.1)
The vector field $\mathbf{v}$ associated with the above group of transformations can be written as

$$\mathbf{v} = \sum_{i=1}^{n} \xi^i(r,p)\partial_{x^i} + \sum_{\alpha=1}^{m} \eta^\alpha(r,p)\partial_{p^\alpha}. \tag{4.3}$$

Lie group of transformations are such that if p is a solution of system (4.1) then $\check{p}$ is also a solution. The method for finding group symmetry [7] is by finding corresponding infinitesimal generator of Lie group of transformations. This leads to an overdetermined linear system of equations for generators $\xi^i(r,p)$, $\eta^j(r,p)$. The invariance of system (4.1) under the infinitesimal transformations leads to the invariance conditions

$$Pr^{(q)}\mathbf{v}[\Delta_s(r, p^u)] = 0, \quad x = 1, \ldots, l \quad \text{whenever} \quad \Delta_x(r, p^u) = 0 \tag{4.4}$$

where $Pr^{(q)}$ is called q^{th} extended infinitesimal generator of the vector field $\mathbf{v}$ given by

$$Pr^{(q)}\mathbf{v} = \mathbf{v} + \sum_{\alpha=1}^{n}\sum \eta_\alpha^j(r, p^u)\partial_{p_j^\alpha} \tag{4.5}$$

where $j = (j_1, \ldots, j_k), 1 \le j_k \le n, 1 \le k \le u$, and sum is over all the orders of j's of order $0 < j \le u$. If j=k, the coefficients η_α^j of $\partial_{p_j^\alpha}$ will depend only on derivatives of p upto order k;

$$\eta_\alpha^j(r, p^u) = D_j\left(\eta_\alpha - \sum_{i=1}^{n}\xi^i p_i^\alpha\right) + \sum_{i=1}^{n}\xi^i p_{j,i}^\alpha \tag{4.6}$$

where $p_i^\alpha = \frac{\partial p^\alpha}{\partial r^i}$, $p_{j,i}^\alpha = \frac{\partial p_i^\alpha}{\partial r^i}$.
To obtain the generators of infinitesimal transformations, substitute equation (4.6) into equation (4.4). The set of all infinitesimal symmetries of this system has an important property that the elements of this set form a Lie algebra under the usual Lie bracket. To reduce primary partial differential equation (PDE) by one independent variable, we find the invariant functions by solving Lagrange's characteristic equations

$$\frac{dr}{\xi^i(r,p)} = \frac{dp}{\eta^j(r,p)}. \tag{4.7}$$

By iterating this process, we get ordinary differential equation from primary equation. Solving an ODE analytically relaively easier that a PDE.

5. Lie symmetry analysis of $(3+1)$-dimensional NLEE

We achieve similarity reductions of the NLEE $(\star)$ using Lie symmetry analysis [7, 8]. The one-parameter Lie group of infinitesimal transformations,

$$\begin{aligned}
\overset{\circ}{\mathrm{r}} &= r + \varsigma\xi^1(r,s,q,t,v) + O(\varsigma^2)\\
\overset{\circ}{\mathrm{s}} &= s + \varsigma\xi^2(r,s,q,t,v) + O(\varsigma^2)\\
\overset{\circ}{\mathrm{q}} &= q + \varsigma\xi^3(r,s,q,t,v) + O(\varsigma^2)\\
\overset{\circ}{\mathrm{t}} &= t + \varsigma\tau(r,s,q,t,v) + O(\varsigma^2)\\
\overset{\circ}{\mathrm{v}} &= v + \varsigma\eta(r,s,q,t,v) + O(\varsigma^2)
\end{aligned} \tag{5.1}$$

where $\xi^1, \xi^2, \xi^3, \tau$ and η are the generators of Lie group transformations with continuous group parameter ς. The associated vector field is represented by

$$\Theta = \xi^1(r,s,q,t,v)\partial_r + \xi^2(r,s,q,t,v)\partial_s + \xi^3(r,s,q,t,v)\partial_q + \tau(r,s,q,t,v)\partial_t + \eta(r,s,q,t,v)\partial_v.$$

The infinitesimal criteria for the invariance of $(\star)$ is

$$3\eta_{rrq} - 2\eta_{rst} + \eta_{rrrrs} - 2\eta_{rs}v_{rr} - 2\eta_{rr}v_{rs} + 2\eta_{rs}^2 + 2(\eta_s - \eta_r)v_{rrs} + 2\eta_{rrs}(v_s - v_r) = 0 \tag{5.2}$$

which is obtained from the invariance condition, $Pr^{(5)}\Theta(\Delta) = 0$, whenever $\Delta = 0$, where $Pr^{(5)}\Theta$ is fifth prolongation of Θ. We obtain determining equations which are constituted of overdetermined system of coupled partial differential equations (PDEs)

$$\begin{aligned}
&\xi_v^1 = \xi_s^1 = \xi_q^1 = 0,\ \xi_r^1 = \frac{1}{3}\tau_t,\\
&\xi_v^2 = \xi_r^2 = \xi_t^2 = 0,\ \xi_s^2 = \frac{1}{3}\tau_t,\\
&\xi_v^3 = \xi_r^3 = \xi_s^3 = \xi_t^3 = 0,\ \xi_q^2 = \tau_t,\\
&\tau_v = \tau_r = \tau_q = 0 = \tau_s = \tau_{tt},\\
&\eta_v = -\frac{1}{3}\tau_t,\ \eta_r = \eta_s - \frac{3}{2} - \xi_q^2 + \xi_t^1,\ \eta_s s = 0.
\end{aligned} \tag{5.3}$$

Solving determining equations (5.3) yields infinitesimal generators

$$\begin{aligned}
\xi^1 =& \frac{c_1}{3} r + \varphi_2(t) \\
\xi^2 =& \quad \frac{c_1}{3} s + \varphi_1(q) \\
\xi^3 =& \quad c_1 q + c_3 \\
\tau =& \quad c_1 t + c_2 \\
\eta =& -\frac{c_1}{3} v - \frac{3}{2} r \varphi_1'(q) + r \varphi_2'(t) + (r+s)\varphi_3(q,t) + \varphi_4(q,t)
\end{aligned} \tag{5.4}$$

where $\varphi_i(,)$, $i = 1, \ldots, 4$ are arbitrary functions for indicated variables and c_i, $i = 1, \ldots, 3$ are arbitrary constants. Assume $\varphi_1(q) = c_4 q$, $\varphi_2(t) = c_5 t$, $\varphi_3(q,t) = c_5$ and $\varphi_4(q,t) = c_6$, the Lie algebra of infinitesimal symmetries of $(\star)$ is spanned by following vector fields

$$\begin{aligned}
\vartheta_1 =& \quad \frac{r}{3}\frac{\partial}{\partial r} + \frac{s}{3}\frac{\partial}{\partial s} + q\frac{\partial}{\partial q} + t\frac{\partial}{\partial t} - \frac{v}{3}\frac{\partial}{\partial v} \\
\vartheta_2 =& \quad \frac{\partial}{\partial t}, \quad \vartheta_3 = \frac{\partial}{\partial q}, \quad \vartheta_4 = q\frac{\partial}{\partial s} - \frac{3}{2} r \frac{\partial}{\partial v}, \\
\vartheta_5 =& \quad t\frac{\partial}{\partial r} + r\frac{\partial}{\partial v}, \quad \vartheta_6 = (r+s)\frac{\partial}{\partial v}, \quad \vartheta_7 = \frac{\partial}{\partial v}.
\end{aligned} \tag{5.5}$$

Lie bracket table having $(i,j)^{th}$ entry $[\vartheta_i, \vartheta_j] = \vartheta_i \cdot \vartheta_j - \vartheta_j \cdot \vartheta_i$ is used to denote commutation relation of Lie algebra. Since $[\vartheta_\alpha, \vartheta_\beta] = -[\vartheta_\beta, \vartheta_\alpha]$, The commutator table is antisymmetric. The structure constants are easily read off from the commutator table.

$*$	ϑ_1	ϑ_2	ϑ_3	ϑ_4	ϑ_5	ϑ_6	ϑ_7
ϑ_1	0	ϑ_2	$-\vartheta_3$	$\frac{2}{3}\vartheta_4$	$\frac{2}{3}\vartheta_5$	$\frac{2}{3}\vartheta_6$	$-\frac{1}{3}\vartheta_7$
ϑ_2	$-\vartheta_2$	0	0	0	ϑ_5	0	0
ϑ_3	ϑ_3	0	0	0	0	0	0
ϑ_4	$-\frac{2}{3}\vartheta_4$	0	0	0	0	0	0
ϑ_5	$-\frac{2}{3}\vartheta_5$	ϑ_5	0	0	0	ϑ_7	0
ϑ_6	$-\frac{2}{3}\vartheta_6$	0	0	0	$-\vartheta_7$	0	0
ϑ_7	$\frac{1}{3}\vartheta_7$	0	0	0	0	0	0

As depicted in the table above, the generalized (3+1)-dimensional NLEE contains a continuous group of transformations which is generated by the infinite-dimensional Lie algebra spanned by vector fields (5.5). Since the infinite number of subalgebras for this Lie algebra is constituted from linear combinations of generators, in our case $\vartheta_i, i = 1, 2, \ldots, 7$.

6. Symmetry reduction and soliton solutions

In this section, we obtain group invariant solutions for Eq.$(\star)$ from the reduction equations. The reduction equations can be found with the assistance of invariant functions. Therefore, first we solve associated Lagrange's system to find invariant functions which are the constant of integration of the characteristic equations

$$\frac{dx}{\xi^1(r,s,q,t,v)} = \frac{dy}{\xi^2(r,s,q,t,v)} = \frac{dz}{\xi^3(r,s,q,t,v)} = \frac{dt}{\tau(r,s,q,t,v)} = \frac{dv}{\eta(r,s,q,t,v)}. \tag{6.1}$$

Invariant functions acquired from these characteristic equations assist to construct invariant solutions. Group invariant solutions are characterized by their invariance under the Lie symmetry group of a PDE. The solutions which are invariant

under one-parameter Lie group can be found by solving the system of differential equations involving one-less independent variable than the original equation.

6.1. **Vector field ϑ_1.**

$$\vartheta_1 = \quad \frac{r}{3}\frac{\partial}{\partial r} + \frac{s}{3}\frac{\partial}{\partial s} + q\frac{\partial}{\partial q} + t\frac{\partial}{\partial t} - \frac{v}{3}\frac{\partial}{\partial v} \tag{6.2}$$

The Lagrange's system of characteristic equations for the vector field ϑ_1 are given by

$$\frac{dr}{\frac{r}{3}} = \frac{ds}{\frac{s}{3}} = \frac{dq}{q} = \frac{dt}{t} = \frac{dv}{-\frac{v}{3}}$$

The invariant functions generated by similarity reduction of Eq. ($\star$),

$$v(r,s,q,t) = \frac{f(R,S,Q)}{t^{\frac{1}{3}}}, \quad \text{where} \quad R = \frac{r}{t^{\frac{1}{3}}}, \quad S = \frac{s}{t^{\frac{1}{3}}} \quad \text{and} \quad Q = \frac{q}{t}. \tag{6.3}$$

Imputing values from Eq. (6.3) into Eq. ($\star$), we obtain the following PDE

$$2f_{RS}^2 - 2f_{RS}f_{RR} + 3f_{RRQ} + 2(f_S - f_R)f_{RRS} + 2f_{RS} + Zf_{RSQ} - \frac{f_{RSS}}{3} - \frac{R}{3}f_{RRS} + f_{RRRRS} = 0. \tag{6.4}$$

Applying similarity transformation method on Eq.(6.4), we obtain following infinitesimal generators

$$\begin{aligned}
\xi_R &= a_2 \\
\xi_S &= \frac{a_1}{Q^{\frac{1}{3}}} \\
\xi_Q &= 0 \\
\eta_f &= -\frac{a_2 R}{6} + \psi_1(Q)S + R\psi_1(Q) + R\frac{a_1}{2Q^{\frac{4}{3}}} + \psi_2(Q) - \frac{a_2 R}{2Q^{\frac{4}{3}}}
\end{aligned}$$

where ξ_R, ξ_S, ξ_Q and η_f denote infinitesimal generators with respect to indicated variable. a_1 and a_2 are arbitrary constants and $\psi_i(Q)$, $i = 1, 2$ are arbitrary functions.
Case 1: $a_1 \neq 0$ and else parameters and arbitrary functions are zero.
Using Lagrange's characteristic equations, the function f with new similarity x and y can be written as

$$f(R,S,Q) = \frac{RS}{2Q} + H(x,y), \quad \text{where} \quad x = R \quad \text{and} \quad y = Q \tag{6.5}$$

The Eq. (6.4) is reduced into the following PDE

$$-\frac{1}{y^2} - \frac{1}{y}H_{xx} + \frac{1}{2y} = 0. \tag{6.6}$$

The solution of equation of equation ($\star$) is

$$v(r,s,q,t) = \frac{r^2}{2z} + \frac{r^2}{4t} + \frac{r}{t^{\frac{2}{3}}}\alpha_1\left(\frac{q}{t}\right) + \frac{1}{t^{\frac{1}{3}}}\alpha_2\left(\frac{q}{t}\right) \tag{6.7}$$

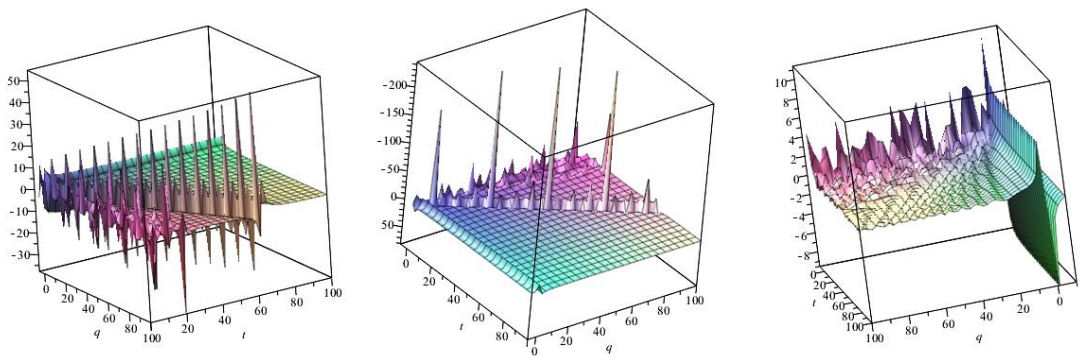

(A) (B) (C)

FIGURE 1. Interaction of dark and bright soliton for Eq. ($\star$). **(A)** $\alpha_1(\frac{q}{t}) = \alpha_2(\frac{q}{t}) = \sec(\frac{q}{t})$, $q \in [-5, 100]$, $t \in [0, 100]$, **(B)** $\alpha_1(\frac{q}{t}) = \alpha_2(\frac{q}{t}) = \sec(\frac{q}{t})$, $q,\ t \in [-5, 10]$, **(C)** $\alpha_1(\frac{q}{t}) = \sin(\frac{q^2}{t})$, $\alpha_2(\frac{q}{t}) = \cos(\frac{q^2}{t})$, $q,\ t \in [-5, 100]$.

Fig. (1) of Eq. (6.7) exhibits bright solitons and dark solitons. Fig.(1)(C) illustrates the interactions between evolving multi-soliton complexes and partially traveling & partially standing waves. This incoherent beam dynamics is diagonally positioned wherein complexes are differentially reaching at cusp of partially travelling component of standing wave. Thus, swell propagation has a evolving trend.

Note that elastic arteries do not change their volume within the physiological range of deformation exerted by pressure gradient force. Thus, elastic arteries can be regarded as incompressible materials. The axisymmetric elastic artery under inflation stress retains its vessel wall structure, whereas a non-axisymmetric elastic artery under inflation stress develops significant shear stresses due to propagation of solitary waves radiating toward the tunica media. The cyclical interaction among solitons introduces quasi-static process on the vessel wall. Note that other than soliton interaction, the impact on aortic vessel wall depends on systolic & diastolic blood pressure, partial pressure of oxygen & carbon dioxide, and monosaccharide concentration.

6.2. **Vector field ϑ_2.**

$$\vartheta_2 = \quad \frac{\partial}{\partial t},$$

The similarity reduction of Eq. ($\star$) is obtained by solving Lagrange's characteristic equations (6.1)

$$v(r, s, q, t) = f(R, S, Q), \quad \text{where} \quad R = r, \quad S = s, \quad \text{and} \quad Q = q. \tag{6.8}$$

We obtain following PDE using Eqs. (6.8) and ($\star$),

$$3f_{RRQ} + f_{RRRRS} - 2f_{RR}f_{RS} + 2f_{RS}^2 + (f_S - f_R)f_{RRS} = 0. \tag{6.9}$$

Travelling wave solutions of Eq. (6.9) is

$$f(R, S, Q) = \frac{-6C_2^2 \tanh(C_2R + C_4S - \frac{4}{3}C_2^2C_4Q + C_1)}{C_2 - C_4} + C_5 \tag{6.10}$$

The solutions of Eq. ($\star$) are

$$v(r, s, q, t) = \frac{-6C_2^2 \tanh(C_2r + C_4s - \frac{4}{3}C_2^2C_4q + C_1)}{C_2 - C_4} + C_5 \tag{6.11}$$

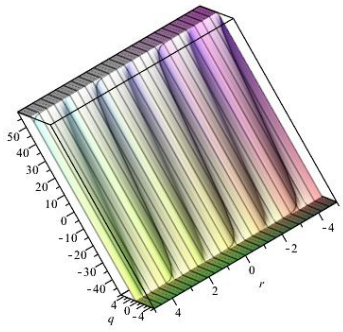

(A)

FIGURE 2. Traveling wave solution (6.11) for Eq. ($\star$), with $s = 1.0885$ and $C_1 = 1,\ C_2 = 3,\ C_4 = 2,\ C_5 = 5$

Fig. (2) of Eq. (6.11) shows a treveling wave. It is characterized by periodic disturbance that moves through the medium. It is worth stating that individual atoms of the medium does not change the position but oscillate at their primal position. It is illustrated that blood flow at mean blood pressure, 100 mm Hg, is propagated forward with each left ventricular contraction. It is inferred that asymptotically biomechanical characteristics of vessel wall of the aorta will remain incompressible and hence, flows will be newtonian in aorta.

Now, we find a new set of infinitesimal generator for Eq. (6.9)

$$\begin{aligned} \xi_R &= \frac{a_1}{3}R + a_3 \\ \xi_S &= \frac{a_1}{3}S + \alpha_1(Q) \\ \xi_Q &= a_1 Q + a_2 \\ \eta_f &= \frac{-a_1}{3}f - \frac{3}{2}R\alpha_1'(Q) + (R+S)\alpha_2(Q) + \alpha_3(Q). \end{aligned} \tag{6.12}$$

where $\xi_R,\ \xi_S,\ \xi_Q$ and η_f denote infinitesimal generators with respect to indicated variable. $\alpha_i,\ i = 1, 2, 3$ are arbitrary functions of Q and $a_1,\ a_2$ & a_3 are arbitrary constants. Assume $\alpha_(Q) = a_4$.

Case 1: $a_1 \neq 0$, remaining arbitrary parameter and functions are zero.

On solving Lagrange's equations, the new similarity form for f is given by

$$f(R, S, Q) = \frac{H(x, y)}{Q^{\frac{1}{3}}}, \text{and} \quad x = \frac{R}{Q^{\frac{1}{3}}}, \quad y = \frac{S}{Q^{\frac{1}{3}}}. \tag{6.13}$$

where x and y are similarity variables. Equation (6.9) can be reduced into following PDE as follows:

$$2H_{xy}^2 - 2H_{xy}H_{xx} + 2(H_y - H_x)H_{xxy} - 3H_{xx} - yH_{xxy} - xH_{xxx} + H_{xxxxy} = 0 \tag{6.14}$$

Generators of infinitesimal transformations for Eq. (6.14) are

$$\xi_x = 0,\ \xi_y = b_1,\ \eta_H = -\frac{b_1}{2} + (x + y)b_2 + b_3 \tag{6.15}$$

The function H in the similarity form can be written as

$$H(x, y) = -\frac{xy}{2} + \left(xy + \frac{y^2}{2}\right)\frac{b_2}{b_1} + \frac{b_3}{b_1}y + G(\zeta), \quad \& \quad \zeta = x \tag{6.16}$$

The reduced form of Eq. $(\star)$ is

$$2\left(\frac{1}{2}+\frac{b_2}{b_1}\right)^2-2\left(\frac{1}{2}+\frac{b_2}{b_1}\right)G''(\zeta)-3G''(\zeta)-\zeta G'''(\zeta)=0 \tag{6.17}$$

Solutions of this ODE is

$$G(\zeta)=\frac{1}{2b_1(b_1\zeta+b_1+2b_2)}+\frac{(b_1+2b_2)^2\zeta^2}{12b_1^2}+b_1\zeta+C_1. \tag{6.18}$$

$$v(r,s,q,t)=-\frac{rs}{2q}+\frac{b_2}{b_1}\left(\frac{rs}{q}+\frac{s^2}{2q}\right)+\frac{b_3}{b_1}\frac{s}{q^{\frac{2}{3}}}+\frac{1}{2b_1(b_1r+b_1q^{\frac{1}{3}}+2b_2q^{\frac{1}{3}})}+\frac{(b_1+2b_2)^2r^2}{12b_1^2q}+b_1\frac{r}{q^{\frac{2}{3}}}+C_1. \tag{6.19}$$

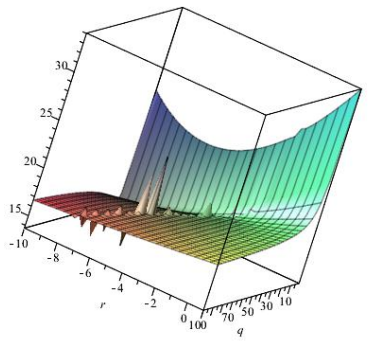

(A)

FIGURE 3. Bright and dark solitons for (6.19), with $b_1 = 4.320,\ b_2 = 1.2758,\ b_3 = 0.5866,\ C_1 = 18$ and $r \in [-10, 1],\ q \in [1, 100]$

Fig. (3) of Eq. (6.19) exhibits bright solitons and dark solitons. It is shown that bright soliton causes temporary increments in amplitude of associative wave than the background whereas dark soliton relatively reduces the intensity than the background in a continuous time beam. Since coherence among bright soliton and dark soliton is diagonal, the scale in the crested direction becomes finite wherein, consequently beam dynamics occurs. Representation in tandem is suggestive of perfectly elastic collisions. Note that after collision between bright soliton and dark soliton, the small-amplitude solitons dark solitons propagate faster than the large-amplitude solitons bright solitons. The axisymmetric characteristic of vessel wall of aorta is owing to coupling of left ventricular ejection fraction per systole. However, due to degenerative changes including cystic medial necrosis, atherosclerosis with/without calcific deposits makes vessel wall of the aorta non-axisymmetric that decouples heart-aorta. In such situation, multiple solitons are generated and their interaction ensues. Such aortic rigidity allows interactions in more than one coordinate that might result into unstable wave field.

Case 2: $a_4 \neq 0$, remaining arbitrary parameter and functions are zero.
The associated Lagrange' system is the associated Lagrange's characteristic equations reduce the function f in new similarity form as

$$f(R,S,Q)=\frac{-3RS}{2Q}+H(x,y), \text{and} \quad x=R, \quad y=Q. \tag{6.20}$$

we reduce Eq. (6.9) into following PDE

$$3H_{xxy} + 3H_{xx} + \frac{9}{2y} = 0 \tag{6.21}$$

The solution of Eq. (6.21) is

$$H(x,y) = \alpha_1(y) + \alpha_2(y)x - \frac{3x^2}{4} - \frac{x}{y}\alpha_3(x) + \frac{1}{y}\int x\alpha_3(x)dr. \tag{6.22}$$

By back substitution, Solution of Eq. $(\star)$ is given by

$$v(r,s,q,t) = \alpha_1(q) + \alpha_2(q)r - \frac{3r^2}{4} - \frac{r}{q}\alpha_3(r) + \frac{1}{q}\int r\alpha_3(r)dr. \tag{6.23}$$

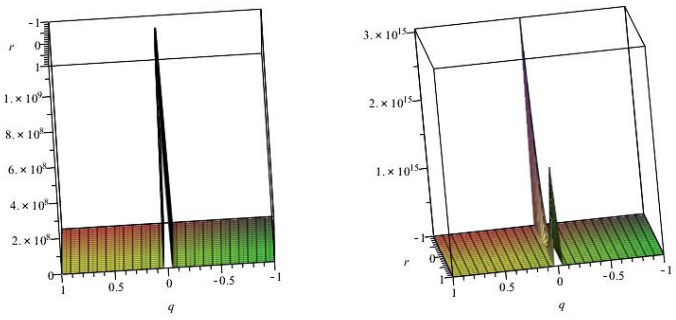

(A) (B)

FIGURE 4. Peregrine soliton (6.23) for Eq. $(\star)$, with **(A)** $\alpha_1(q) = \sin(q),\ \alpha_2(q) = q,\ \alpha_3(r) = \sec(r)$ and **(B)** $\alpha_1(q) = \sec(q),\ \alpha_2(q) = q,\ \alpha_3(r) = \sin(r),\ r,\ q \in [-1,1]$.

Figure (4) shows the Peregrine soliton, a localized nonlinear structure with strong temporal and spatial localization. Our result do not correspond to mathematical ideal Peregrine soliton characteristics. The progressive and concomitant increase in temporal localization as well as increase in spatial localization is associated with Peregrine soliton characteristics. Asymptotically, this progressive increase contributes to modulation-instability recurrence period. The periodic loading of porous dispersive media, the tunica media, leads to stress softening of wall material. Nearly repetitive cyclic loading of the tunica media by Peregrine soliton contributes to injury to vessel wall. In a dissipative system, this deformation process is associated with elastoplastic effects leading to significant vessel wall injury. Peregrine soliton impact aortic root would cause aortic valvular insufficiency through regurgitation of blood into left ventricle and pericardium causing pericardiac tamponade.

6.3. **Vector field ϑ_3.**

$$\vartheta_3 = \frac{\partial}{\partial q}$$

The similarity reduction of Eq. $(\star)$ is obtained by solving Lagrange's system of characteristic equations (6.1)

$$v(r,s,q,t) = f(R,S,T), \qquad R = r, \quad S = s \quad \text{and} \quad T = t. \tag{6.24}$$

From Eqs. (6.24) and $(\star)$, we obtain PDE

$$-2f_{RST} + f_{RRRRS} - 2f_{RR}f_{RS} + 2f_{RS}^2 + 2(f_S - f_R)f_{RRS} = 0. \tag{6.25}$$

The new set of infinitesimal generator for Eq. (6.25) by applying similarity transformation method is

$$\begin{aligned}\xi_R &= \frac{a_1}{3}R + \alpha_1(T),\\ \xi_S &= \frac{a_1}{3}S + a_3,\\ \tau_T &= a_1 T + a_2,\\ \eta_f &= -\frac{a_1}{3}f + (R+S)\alpha_2(T) + R\alpha_1'(T) + \alpha_3(T).\end{aligned}$$

where a_i, $i = 1, \ldots, 3$ are arbitrary constants. Assume $\alpha_1(T) = a_4$..
Case 1: $a_1 \neq 0$, remaining arbitrary parameters and functions are zero.
By solving Lagrange's characteristic equations, we can write f in the term of new similarity solution with $x,\ y$

$$f(R,S,T) = \frac{H(x,y)}{T^{\frac{1}{3}}}, \quad \text{where} \quad x = \frac{R}{T^{\frac{1}{3}}} \quad \text{and} \quad y = \frac{S}{T^{\frac{1}{3}}}. \tag{6.26}$$

Further, Eq. (6.25) can be reduced into following PDE as follows:

$$2H_{xy}^2 - 4H_{xx}H_{xy} + 2(H_y - H_x)H_{xxy} - 2H_{xy} - \frac{2}{3}yH_{xyy} - \frac{2}{3}xH_{xxy} + H_{xxxxy} = 0 \tag{6.27}$$

The solution of PDE (6.27) is given by

$$H(x,y) = \lambda(x) + \mu(y) \tag{6.28}$$

Hence, the solution of primary equation ($\star$) is

$$v(r,s,q,t) = \frac{1}{t^{\frac{1}{3}}}\left[\lambda\left(\frac{r}{t^{\frac{1}{3}}}\right) + \mu\left(\frac{s}{t^{\frac{1}{3}}}\right)\right]. \tag{6.29}$$

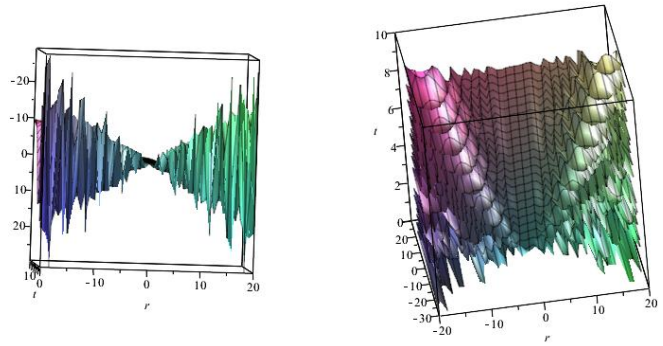

(A) (B)

FIGURE 5. Breathers (6.29) for Eq. ($\star$) with $r \in [-20, 20]$, $t \in [0, 10]$ **(A)**$\lambda(\frac{r}{t^{\frac{1}{3}}}) = r\sin(\frac{r}{t^{\frac{2}{3}}})$, $\mu(\frac{s}{t^{\frac{1}{3}}}) = \frac{(0.0235)^3}{t}$, **(B)** $\lambda(\frac{r}{t^{\frac{1}{3}}}) = r\sin(\frac{r^2}{t^{\frac{2}{3}}})$, $\mu(\frac{s}{t^{\frac{1}{3}}}) = \frac{(0.0235)^3}{t}$.

Figure (5) exhibits breather solutions. A breather is a nonlinear wave wherein, energy concentrate in local and oscillatory manner. Standing breathers are localized solution with varying amplitude. The general breather solutions can be derived by defining appropriate parameters in Eq. (6.29), their corresponding dynamical behavior is represented in Fig. (5). Both

of these breathers are periodic in space directions as well as localized in time directions. It is shown that the solitary wave generated in the center of aorta axially, the pressure reaction force can generate compression waves impacting the vessel wall of the aorta. Note that the localization characteristic of breather has different impact on different dimension resulting into differential strain energy density functions.

Case 2: $a_2 \neq 0$, remaining arbitrary parameters and functions are zero.

The function f in the form of new similarity solution $H(x, y)$ is

$$f(R, S, T) = H(x, y), \quad \text{where} \quad x = R \quad \text{and} \quad y = S. \tag{6.30}$$

Equation (6.25) can be reduced into PDE

$$H_{xxxxy} - 2H_{xy}H_{xx} + 2H_{xy}^2 + 2(H_y - H_x)H_{xxy} = 0 \tag{6.31}$$

The solution of Eq.(6.31) provide following solution of Eq. $(\star)$

$$v(r, s, q, t) = \lambda(r) + \mu(s) \tag{6.32}$$

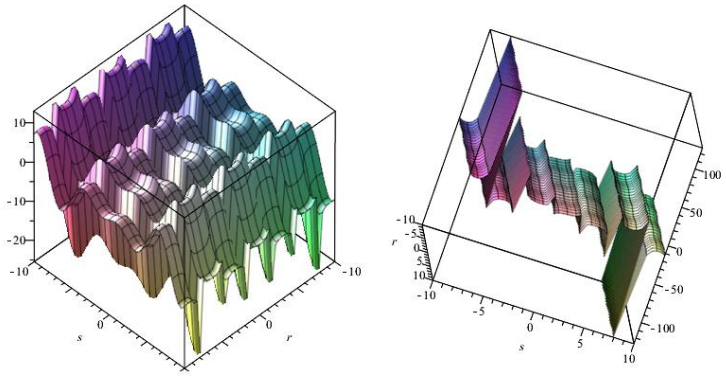

(A) (B)

FIGURE 6. Rogue wave solution (6.32) for Eq. $(\star)$, with $r,\ s \in [-10, 10]$, **(A)**$\lambda(r) = \sec(r),\ \mu(s) = s\cos(s)$, **(B)**$\lambda(r) = \sin(r),\ \mu(s) = s\sec(s)$.

Interactions among fundamental solitons in terms of mutual collisions and mutual amplifications contributes to formation of rogue wave as shown in Fig. (6). The granularity and inhomogeneity of fundamental solitons are considered as joint generators of rogue waves in vitro. The spectrum of rogue waves can not be characterize by finite width and modulation stability analysis. Non-homogeneous perturbations and multi-directional spreading causes rogue wave formation. The concentrically arranged elastic fibrils have a statistically distributed initial length. Each fibril can be stretched with very low impact of singular soliton, but thereafter further stretching of fibril is linearly elastic and impact on tunica media linearly.

6.4. **Vector field ϑ_4.**

$$\vartheta_5 = q\frac{\partial}{\partial s} - \frac{3r}{2}\frac{\partial}{\partial v}. \tag{6.33}$$

Equation $(\star)$ can be reduced into the following similarity form with new similarity variables

$$v(r, s, q, t) = -\frac{3rs}{2q} + f(R, Q, T) \quad \text{where} \quad R = r, \quad Q = q \quad \text{and} \quad T = t. \tag{6.34}$$

We obtain the following PDE from Eqs. (6.34) and ($\star$)

$$3f_{RRQ} + \frac{3}{Q}f_{RR} + \frac{9}{2Q^2} = 0. \tag{6.35}$$

The solution of Eq. (6.35) is

$$f(R,Q,T) = \lambda_1(Q,T) + \lambda_(Q,T)R - \frac{3R^2\log(Q)}{4Q} - \frac{R}{Q}\lambda_3(R,T) + \frac{1}{Q}\int R\lambda_3(R,T)dR \tag{6.36}$$

Following solution of the primary Eq. ($\star$) is,

$$v(r,s,q,t) = \lambda_1(q,t) + \lambda_(q,t)r - \frac{3r^2\log(q)}{4q} - \frac{r}{q}\lambda_3(r,t) + \frac{1}{q}\int r\lambda_3(r,t)dr, \tag{6.37}$$

where $\lambda_i(,)$ are some arbitrary functions.

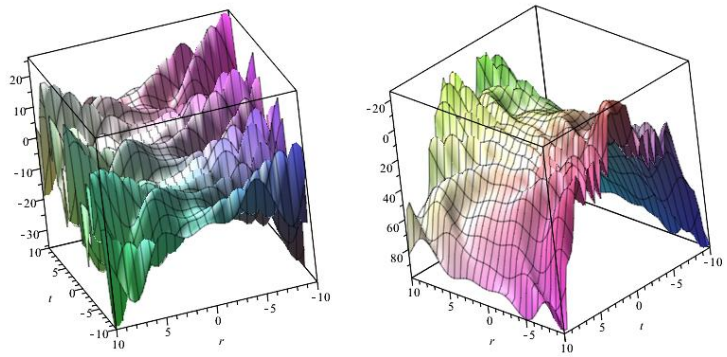

(A) (B)

FIGURE 7. Multi-soliton complex for Eq. ($\star$) with $r,\ t \in [-10,10]$, $q = 1.087$ **(A)** $\lambda_1(q,t) = t\sin(q)$, $\lambda_2(q,t) = q\cos(t)$, $\lambda_3(r,t) = t\sin(r+t^2)$, **(B)** $\lambda_1(q,t) = t^2\sin(q)$, $\lambda_2(q,t) = q\cos(t)$, $\lambda_3(r,t) = t\sin(r+t^2)$.

Figure (7) shows multi-soliton complex solution (6.37). It is a self localized state wherein, several fundamental soliton including bright solitons and dark solitons are nonlinearly superimposed. Asymptotically, such nonlinear superimposition can be either coherent or incoherent resulting into either independent or dependent phases of separate soliton. Essentially it is a parametric interaction among waves at different frequencies having constructive and destructive interactions. The mixed polarization of fundamental solitons characteristically captures coherent and incoherent soliton interactions. Note that pair-wise collisions reshape multi-soliton complexes but complexes do not radiate. Due to incoherent and coherent interactions among multi-soliton complexes significant positive as well as negative impact occur to vessel wall of the aorta through dynamic pathology. The destructive effect of wave resonance include initial intimal flap injury.

7. Conclusion

To depict role of interactions among fundamental solitons, we formulated a generalized (3+1)-dimensional nonlinear evolution equation. To seek representative examples of solitons, we obtained the infinitesimal generators, commutator table of Lie algebra, symmetry groups for the nonlinear evolution equation. By using Lie group of transformations method, similarity reduction is conducted to find invariant solutions for NLEE.

The abnormal aortic wave reflections are responsible for pathological aortic wave. The soliton waves emerging from more than one coordinate (q,t), (r,s) and (r,t) results into unstable wave field and generation of pathological waves. Due to complex soliton interaction, forward waves toward common iliac arteries and backward waves toward left ventricle. Within physiological exercise tolerance threshold, the cardiac output operates close to upper boundary value, such cardiac overloading due to exercise can reduce the threshold for the occurrence myocardial ischemia. Similarly, a boundary value exist for vessel wall of the aorta. Hence, progressive increase in the strain to tunica media through tunica intima reduce threshold for injury to tunica intima and thereon permeation of blood into tunica media ensues. Thus, the formation of dynamic pathology contributes to sudden rupture, torrential bleed and death. The degenerative changes including atherosclerosis with subintimal calcium deposits and elevated systolic blood pressure hardens the vessel wall of the aorta. Under normal conditions, the pulsatile cardiac output is optimized by arterial wave reflection. But with progressive hardening of vessel wall of the aorta, the optimum cardiac output is minimized since the aortic rigidity increases. Also, the pressure gradient force applied to the vessel wall increases with higher value of aortic rigidity. Both of the above factors contributes to progression of aortic dissection. Note that pathological aortic waves can be created without any anatomical and/or physiological abnormalities. Also, cardiovascular diseases alters coronary microvasculature-heart-lung- aorta and its great vessels dynamics and create pathological waves. This dynamic pathology as a pathological waves can cause aneurysmal rupture as well as progression of aortic dissection.

7.1. **Future Scope.** : Our work will enable experimental scientists to design deep-water wave basins and wave guage measurements to simulate aortic dissection and design experiment to observe diagonal hydrodynamic solution that might help to replicate bright, dark and Peregrine solitons. Multiscale modeling of heart-aorta coupling can help to detect dynamic pathology in aorta. Using data science, this can be done for individual patient without anatomical and/or physiological deficit. Thus, it can help cardiothoracic physicians to identify latent cases and start preventive regimen including control of hypertension and restriction on physiological activity.

Compliance with ethical standards
Conflict of interest The authors declare no conflict of interest.

Data Availability Statement
All data generated or analysed during this study is included in this article.

References

[1] Hirota, R.: The Direct Method in Soliton Theory. Cambridge University Press, Cambridge (2004).
[2] Matveev, V.B., Salle, M.A.: Darboux Transformation and Solitons. Springer, Berlin (1991).
[3] M. J. Ablowitz and P. A. Clarkson, *Solitons, nonlinear evolution equations and inverse scattering*, London Mathematical Society Lecture Note Series, 149, Cambridge University Press, Cambridge, (1991).
[4] M. Wang, X. Li and J. Zhang, The $(\frac{G'}{G})$-expansion method and travelling wave solutions of nonlinear evolution equations in mathematical physics, Phys. Lett. A **372** (2008), no. 4, 417–423.
[5] C. Rogers and W. F. Shadwick, *Bäcklund transformations and their applications*, Mathematics in Science and Engineering, 161, Academic Press, Inc., New York, (1982).
[6] *Bäcklund transformations, the inverse scattering method, solitons, and their applications*, Lecture Notes in Mathematics, Vol. 515, Springer-Verlag, Berlin, (1976).
[7] G. W. Bluman and S. Kumei, *Symmetries and differential equations*, Applied Mathematical Sciences, 81, Springer-Verlag, New York, (1989).
[8] P. J. Olver, *Applications of Lie groups to differential equations*, second edition, Graduate Texts in Mathematics, 107, Springer-Verlag, New York, (1993).
[9] J. J. Boyle, P. L. Weissberg, and M. R. Bennett, Tumor necrosis factor- promotes macrophage-induced vascular smooth muscle cell apoptosis by direct and autocrine mechanisms, Arterioscler. Thromb. Vasc. Biol., **23** (2003), 1553–1558.
[10] X. Ju, et al. IL-6 regulates extracellular matrix remodeling associated with aortic dilation in a fibrillin-1 hypomorphic mgR/mgR mouse model of severe Marfan syndrome, J. Am. Heart Assoc., **3** (2014), e000476.

[11] C. A. Nienaber and K. A. Eagle, Aortic dissection: new frontiers in diagnosis and management: part II:therapeutic management and follow-up, Circulation, **108** (2003), 772–778.
[12] R. E. Clough, M. Waltham, D. Giese, P. R. Taylor and T. Schaeffter, A new imaging method for assessment of aortic dissection using four-dimensional phase contrast magnetic resonance imaging, J. Vasc. Surg, **55** (2012), 914–923.
[13] T. Frauenfelder, et al. Triple rule-out CT in the emergency department: protocols and spectrum of imaging findings, Eur. Radiol, **19** (2009), 789–799.
[14] A.G. Moore, et al., Choice of computed tomography, transesophageal echocardiography, magnetic resonance imaging, and aortography in acute aortic dissection: International Registry of Acute Aortic Dissection (IRAD), Am. J. Cardiol, **89**,(2002), 1235–1238.
[15] J. A. Elefteriades, et al., Indications and imaging for aortic surgery: size and other matters, J. Thorac Cardiovasc. Surg, **149** (2015), S10–S13.
[16] A. Redheuil, et al., Age-related changes in aortic arch geometry: relationship with proximal aortic function and left ventricular mass and remodeling, J. Am. Coll. Cardiol, **58** (2011), 1262–1270.
[17] F. A. Lederle, et al., Variability in measurement of abdominal aortic aneurysms, Abdominal Aortic Aneurysm Detection and Management Veterans Administration Cooperative Study Group, J. Vasc. Surg, **21** (1995), 945–952.
[18] N. S. Cayne, et al., Variability of maximal aortic aneurysm diameter measurements on CT scan: significance and methods to minimize, J. Vasc. Surg., **39** (2004), 811–815.
[19] D. Wen, X. Du, J.Z. Dong, X.L. Zhou, and C.S. Ma, Value of D-dimer and C reactive protein in predicting in hospital death in acute aortic dissection, Heart **99** (2013), 1192–1197.
[20] N. Okina, et al. Utility of measuring C-reactive protein for prediction of in-hospital events in patients with acute aortic dissection, Heart Vessels, **28** (2013), 330–335.
[21] A.I. Hickerson, M. Gharib, On the resonance of a pliant tube as a mechanism for valveless pumping, J Fluid Mech,**555** (2006), 141–8.
[22] I. Avrahami, M. Gharib, Computational studies of resonance wave pumping in compliant tubes, J Fluid Mech, **608** (2008), 139–60.
[23] M. Zamir, *The physics of pulsatile flow*, New York: Springer-Verlag, (2000).
[24] A.S. Forouhar, et al, The embryonic vertebrate heart tube is a dynamic suction pump, Science, **312** (2006), 751–3.
[25] G. Liebau, On a valveless pump principle (Ger), Naturwissenschaften, **327**, (1954).
[26] A. Hickerson, D. Rinderknecht, M. Gharib, Experimental study of the behavior of a valveless impedance pump, Exp Fluids, **38** (2005), 534–540.
[27] J.A. Meier, A novel experimental study of a valveless impedance pump for applications at lab-on-chip, microfluidic, and biomedical device size scales, California Institute of Technology, (2011).
[28] M. Zamir, *The physics of coronary blood flow*, Springer Science & Business Media, (2006).
[29] U.F. Pinho, A.V. Babanin, Emergence of short crestedness in originally unidirectional nonlinear waves, Geophys Res Lett, **42** (2015), 4110–4115.
[30] H. Demiray, The effect of shear stress on solitary waves in arteries, Bulletin of mathematical biology, **59** (1997), no. 5, 993–1012.
[31] V. Jadaun and N. R. Singh, *Mathematical Modeling and Well-Posedness of Three-Dimensional Shell in Disorders of Human Vascular System In Nonlinear Systems-Theoretical Aspects and Recent Applications*, IntechOpen,(2020).
[32] W.R. Milnor and M.D. Baltimore,*Haemodynamics*, Williams & Wilkins Co, (1989).
[33] C.M. Quick, D.S. Berger and A. Noordergraaf, Constructive and destructive addition of forward and reflected arterial pulse waves, Am J Physiol Heart Circ Physiol, **280** (2001), H27–H1519.
[34] L. Wang et al., Breather interactions and higher-order nonautonomous rogue waves for the inhomogeneous nonlinear Schrodinger Maxwell-Bloch equations, Ann. Physics 359 (2015), 97–114.
[35] J. Chai et al., Conservation laws, bilinear Backlund transformations and solitons for a nonautonomous nonlinear Schrodinger equation with external potentials, Commun. Nonlinear Sci. Numer. Simul. **39** (2016), 472–480.
[36] V. Jadaun and N. R. Singh, Soliton solutions of generalized (3 + 1)-dimensional Yu-Toda-Sasa-Fukuyama equation using Lie symmetry analysis, Anal. Math. Phys. **10** (2020), no. 4, Paper No. 42, 24 pp.
[37] V. Jadaun and S. Kumar, Symmetry analysis and invariant solutions of (3 + 1)-dimensional Kadomtsev-Petviashvili equation, Int. J. Geom. Methods Mod. Phys. 15 (2018), no. 8, 1850125, 19 pp.
[38] H.-H. Zhao, X.-J. Zhao and H.-Q. Hao, Breather-to-soliton conversions and nonlinear wave interactions in a coupled Hirota system, Appl. Math. Lett. 61 (2016), 8–12.
[39] V. Jadaun and S. Kumar, Lie symmetry analysis and invariant solutions of (3+1)-dimensional Calogero-BogoyavlenskiiSchiff equation, Nonlinear Dyn, 93 (2018), no. 5, 349–360.
[40] T. Dauxois and M. Peyrard, *Physics of solitons*, reprint of the 2006 edition, revised translation of the 2004 French edition, Cambridge University Press, Cambridge, 2010.
[41] V. Jadaun, Phys. Scr. https://doi.org/10.1088/1402-4896/ac0031, (2021).
[42] D. K. Campbell, S. Flach, and Y. S. Kivshar, Localizing energy through nonlinearity and discreteness, Physics Today, **57** (2004), no. 1, 43–49.
[43] F. R. de Hoog, and R. Weiss, The Application of Linear Multistep Methods to Singular Initial Value Problems, Math. Comput., **31** (1977), 676–690.

[44] W. Walter, *Differential and integral inequalities*, Translated from the German by Lisa Rosenblatt and Lawrence Shampine. Ergebnisse der Mathematik und ihrer Grenzgebiete, Band 55, Springer-Verlag, New York, (1970).

Vishakha Jadaun, Department of Mathematics, Netaji Subhas University of Technology, New Delhi-110078, India.
E-mail address, * corresponding author: vishakhasjadaun@gmail.com

Nitin Raja Singh, Department of Management studies, Indian Institute of Technology Delhi, New Delhi-110016, India.
E-mail address: nitinrsingh22@gmail.com